

Linking Natural Oil Seeps from the Gulf of Mexico to Their Origin by Use of Fourier Transform Ion Cyclotron Resonance Mass Spectrometry

Logan C. Krajewski,[†] Vladislav V. Lobodin,^{*,‡} Caroline Johansen,[§] Tessa E. Bartges,[†] Ekaterina V. Maksimova,^{||} Ian R. MacDonald,[§] and Alan G. Marshall^{*,†,‡,||}

[†]Department of Chemistry and Biochemistry, Florida State University, 95 Chieftain Way, Tallahassee, Florida 32306, United States

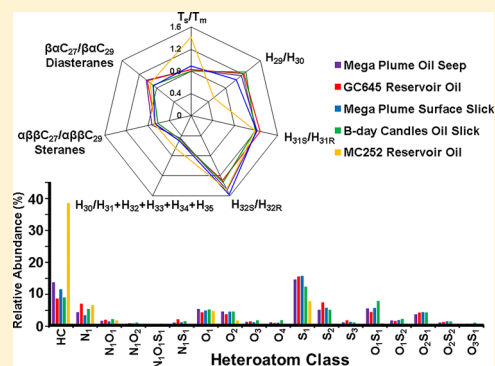
[‡]Ion Cyclotron Resonance Program, National High Magnetic Field Laboratory, Florida State University, 1800 East Paul Dirac Drive, Tallahassee, Florida 32310, United States

[§]Department of Earth, Ocean and Atmospheric Science, Florida State University, 95 Chieftain Way, Tallahassee, Florida 32306, United States

^{||}College of Marine Science, University of South Florida, St. Petersburg, Florida 33701, United States

Supporting Information

ABSTRACT: We report chemical characterization of natural oil seeps from the Gulf of Mexico by Fourier transform ion cyclotron resonance mass spectrometry (FT-ICR MS) and Gas Chromatography/Atmospheric Pressure Chemical Ionization Mass Spectrometry (GC/APCI-MS), to highlight how FT-ICR MS can also be employed as a means to determine petroleum connectivity, in addition to traditional GC/MS techniques. The source of petroleum is the Green Canyon (GC) 600 lease block in the Gulf of Mexico. Within GC600, two natural oil seepage zones, Mega Plume and Birthday Candles, continuously release hydrocarbons and develop persistent oil slicks at the sea surface above them. We chemically trace the petroleum from the surface oil slicks to the Mega Plume seep itself, and further to a petroleum reservoir 5 km away in lease block GC645 (Holstein Reservoir). We establish the connectivity between oil samples and confirm a common geological origin for the oil slicks, oil seep, and reservoir oil. The ratios of seven common petroleum biomarkers detected by GC/APCI-MS display clear similarity between the GC600 and GC645 samples, as well as a distinct difference from another reservoir oil collected ~300 km away (Macondo crude oil from MC252 lease block). FT-ICR MS and principal component analysis (PCA) demonstrate further similarities between the GC600 and GC645 samples that distinctly differ from MC252. A common geographical origin is postulated for the GC600/GC645 samples, with petroleum migrating from the GC645 reservoir to the oil seeps found in GC600 and up through the water column to the sea surface as an oil slick.



INTRODUCTION

Natural oil seeps are global geological features that contribute up to 2 million tonnes of petroleum a year into the environment worldwide, which exceeds all anthropogenic sources combined.^{1,2} The Gulf of Mexico is a prolific oil-producing basin with large oil fields buried kilometers below the sea floor. Oil fields were generated by sediment deposition and drainage from the North American continent,³ and over time the overpressure on the reservoirs caused hydrocarbons to migrate to the sea floor and seep into the water column.^{4,5} There are numerous seepage zones in the Gulf of Mexico, and oil slicks for some of them can be seen on the water surface from space.⁶ The exact volume of petroleum leaked from those seeps is still under debate, with estimated values from 80 000 to 200 000 tonnes annually.² The seep zones are subjects of active ecological^{7–9} and biological^{10–13} studies. Petroleum that enters the environment through these seeps acts as a nutrition source for the local ecosystem¹⁴ that

supports rich biodiversity^{15,16} as it migrates from the reservoir to sea surface. The knowledge of hydrocarbon incorporation into the environment, however, requires familiarity with the connectivity of petroleum from its source to environmental introduction and all points in between. Only then, for example, can the impact of events such as accidental oil spills be fully understood, beyond normal background hydrocarbon incorporation.^{17–19}

To fully describe the fate of a petroleum seep, it must be traced directly to its source reservoir, with oil slicks a typical start point for natural seep detection. Oil on top of the water surface suppresses the surface roughness²⁰ and can be detected by

Received: August 30, 2017

Revised: December 18, 2017

Accepted: December 19, 2017

Published: January 10, 2018

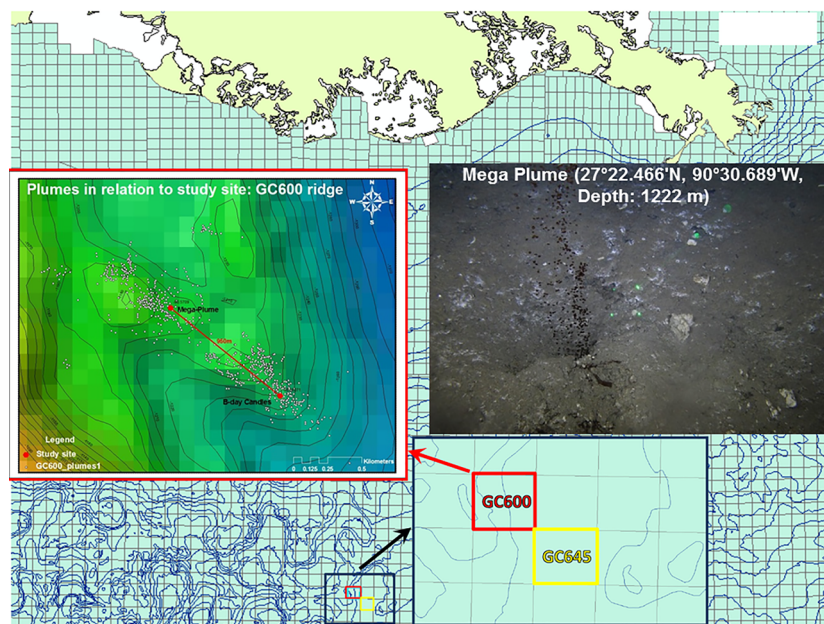


Figure 1. Image of the Gulf of Mexico region off the coast of Louisiana with marked locations of GC600 and GC645 lease blocks. *Inset (left):* Position of “Mega Plume” and “Birthday Candles” oil seeps in GC600. *Inset (right):* Picture of “Mega Plume” oil seep taken at a depth of 1220 m.

satellite radar systems, e.g., synthetic aperture radars (SAR),^{5,21–23} with automated algorithms developed to aid in the detection process.^{24,25} Oil slicks provide an indication of where petroleum directly enters the environment. Video and acoustic methods, along with remotely operated underwater vehicle (ROV) searches, can trace the path of the oil from the seep on the sea floor to the surface.^{26–30} Moreover, these searches may uncover gas hydrate seeps, an indication of an active hydrocarbon system.³¹ Intensive geochemical studies are traditionally implemented after seep discovery to study the migration of the petroleum through fault lines and other natural pathways.^{32–34} Typically, these studies are performed in attempts to determine the location of major source basins, reservoirs, and their maturity.^{35,36} In any case, the evaluation of environmental impact of the petroleum from oil seeps requires understanding of its composition and subsequent transformation. Throughout the migration process from reservoir to surface, the compounds in petroleum are broken up by both microbial activity³⁷ and by weathering effects such as photo-oxidation.^{38,39} The assimilation of petroleum into the environment and the efficiency with which it is environmentally degraded, however, depends on the properties of the oil.⁴⁰ Those properties are in turn governed by the chemical composition of the source reservoir.^{3,41} Environmental transformation is frequently studied to determine the end fate of the oil.⁴²

In this work, we comprehensively analyze oil slicks, oil seeps, and reservoir oil to establish a compositional linkage between the samples and track the transformation of petroleum compounds during migration from the reservoir to the water surface. Biomarker analysis, based on gas chromatography mass spectrometry (GC/MS), has traditionally remained the method of choice for determining relationships between different environmental samples.^{43–46} Sample characterization with this technique remains limited, however, due to the technique’s inability to analyze nonvolatile molecules and limited chromatographic resolution, which traditionally results in a significant unresolved complex mixture (UCM). Here, we employ Fourier

transform ion cyclotron resonance mass spectrometry (FT-ICR MS)^{47–51} to provide chemical fingerprinting information to determine petroleum complexity, while also providing an excellent starting point to begin a more complete characterization of the sample. We examine the petroleum in the Green Canyon (GC) region off the coast of Louisiana, specifically lease block GC600 (Figure 1). We compare samples from oil slicks collected on the water surface sites ~1 km apart to a Mega Plume oil seep sample located in GC600 and to a reservoir sample in nearby lease block GC645 (~5 km SE of GC600), where commercial oil production is being conducted on the Holstein platform. Finally, we compare the samples to a sample from the Macondo reservoir (MC252), approximately 300 km NW of Green Canyon to serve as an experimental control. Although the present methods are previously established, the results represent a novel application of FT-ICR MS to verify chemical connectivity in the environment, supported by traditionally accepted biomarker analysis by gas chromatography/(atmospheric pressure ionization) mass spectrometry (GC/(APCI)-MS).⁵²

■ EXPERIMENTAL METHODS

Sample Collection. U.S. Coast Guard certified Teflon collection nets were used to collect oil samples. Oil was collected from surface slicks at Birthday Candles and Mega Plume by a Teflon net attached to an extractable pole. The oil sample from the Mega Plume seep (27°22.466' N, 90°30.689' W) at depth (~1220 m) was collected by a Teflon net attached to a T-handle which was maneuvered by a remotely operated vehicle (ROV) and then stored in a sealed box on the ROV tray during the ascent. The samples were stored in glass jars at –40 °C. GC645 reservoir oil was provided from the Anadarko operated Holstein Spar oil platform (located approximately 5 km SE from Birthday Candles and Mega Plume). Crude oil from MC252 (NIST2779), 28°44'17.3" N, 88°21'57.4" W, approximately 300 km NW from the natural seep site, was purchased from NIST (Gaithersburg, MD). A description of the samples is given in Table 1.

Sample Preparation. The oiled Teflon mesh (4.1583 g) was washed with 20 mL aliquots of toluene (HPLC grade, J.T. Baker)

Table 1. Sample Description

Mega Plume oil seep	Petroleum collected directly from Mega Plume seep
Mega Plume oil slick	Petroleum collected from oil slick above Mega Plume seep
B-Day Candles oil slick	Petroleum collected from oil slick above B-Day Candles seep
GC645 reservoir	Petroleum collected from Holstein crude reservoir
MC252 reservoir	Petroleum collected from Macondo crude reservoir

until toluene was clear to extract trapped petroleum compounds. The toluene extract was then filtered through a filter paper of medium porosity (Fisher Scientific, Hampton, NH). The filtered extract was evaporated under a gentle nitrogen flow for complete solvent removal and diluted with dichloromethane (HPLC grade, J.T. Baker) to a concentration of 20 mg/mL. Crude oil samples (Holstein and Macondo) were subjected to 5-fold dilution with dichloromethane.

Gas Chromatography/Atmospheric Pressure Chemical Ionization Mass Spectrometry (GC/APCI-MS) and Correlation Analysis. The analysis of petroleum biomarkers was performed with a gas chromatography/atmospheric pressure chemical ionization mass spectrometer (GC/APCI-MS) as described by Lobodin et al.⁵² A GC/APCI-MS instrument consisting of an Agilent 7890 GC system (Agilent Technologies, Santa Clara, CA) and a Xevo TQ-S tandem quadrupole mass spectrometer (Waters Corp., Milford, MA) was equipped with an atmospheric pressure GC ion source. The gas chromatograph parameters were as follows: carrier gas (helium, 99.9995% purity, Airgas, Inc.) at a flow rate of 1.2 mL/min; inlet temperature, 300 °C; oven temperature-programmed from 50 °C for 3 min, then ramped at 20 °C/min to 150 and 2 °C/min from 150 to 350 °C, and then kept at 350 °C for 25 min. A GC column (MXT-5, 60 m long, 250 μm ID, 0.25 μm film thickness) was procured from Restek (Bellefonte, PA). The sample injected volume was 1 μL in split mode (split ratio was 1:10). The transfer line was kept at 350 °C. The ion source was held at 150 °C. Auxiliary gas (250 L/h), cone gas (200 L/h), and makeup gas (350 mL/min) for the APGC ion source was nitrogen delivered from a Dewar (as a boil-off of liquid N₂). Analytes were ionized by APCI (corona discharge in an atmosphere of nitrogen; current, 2.5 μA) and positive ions were mass-analyzed. Argon (99.999% purity, Airgas, Inc.) for collisionally activated dissociation (CAD) was delivered to a collision cell at 0.15 mL/min. Mass spectrometry data were acquired with MassLynx 4.1 software (Waters Corp.) in full scan (*m/z* 50–650) and MS/MS modes: single reaction monitoring (SRM) and product scan. Table S1 shows conditions for acquisition of SRM transitions. Each sample was run in triplicate with a solvent blank between the samples to eliminate carry-over. Areas under biomarker peaks from the corresponding SRM chromatograms were used to calculate biomarker ratios. Seven-axis diagrams were constructed with Microsoft Excel (Microsoft Office Professional Plus 2010). The correlation coefficients were

calculated and plotted with MATLAB R2014a (MathWorks, Natick, MA).

Bulk Elemental Analysis. Elemental analysis was performed as previously described.⁵³ Approximately 1–2 mg of sample was placed in a tin cup for analysis to determine C, H, N, O, and S content. Analysis of 2,5-bis(5-*tert*-butyl-2-benzoxazolyl)-thiophene (BBOT) was performed to provide instrument calibration. To ensure instrument accuracy over time, BBOT was subsequently reanalyzed after the samples.

9.4 T FT-ICR MS. Samples were diluted to 100 μg mL⁻¹ in 50:50 (v/v) toluene/methanol. A custom-built FT-ICR mass spectrometer, with a 22 cm horizontal bore passively shielded 9.4 T magnet, was used for analysis.⁵⁴ Operation and data acquisition were facilitated with a modular ICR data station (Predator).⁵⁵ Ions were generated at atmospheric pressure by direct sample infusion at a rate of 50 μL min⁻¹ into the heated (300 °C) vapor region of an atmospheric pressure photoionization (APPI) source, where gas-phase neutrals, nebulized with the aid of N₂ sheath gas (~50 psi), were photoionized by a 10 eV ultraviolet krypton lamp (Syagen Technology, Inc., Tustin, CA).⁵⁶

Ions were transferred by a tube lens/skimmer into the mass spectrometer, accumulated in an rf-only octopole (100–500 ms), passed through a mass resolving rf-only quadrupole, and collisionally cooled with He gas (~3.5 × 10⁻⁶ Torr). A second rf-octopole transferred the ions into a seven-segment cylindrical ICR detection cell.^{57,58} A broadband frequency sweep (“chirp”) excitation (~70–700 kHz, with sweep rate of 50 Hz/μs and amplitude, V_{p-p} = 0.60 V) was used for detection. A total of 100 time-domain acquisitions were coadded and zero-filled once prior to fast Fourier transform and phase correction to yield an absorption-mode mass spectrum.⁵⁹

Mass Calibration and Data Analysis. ICR frequencies were converted to ion masses based on quadrupolar trapping potential approximation^{60,61} and internally calibrated with a two-step “walking” calibration based on homologous series that differ by degree of alkylation (mass of CH₂).⁶² Ion masses were converted to the Kendrick mass scale, and each assigned a unique elemental composition (C_{*n*}H_{*h*}N_{*n*}O_{*o*}S_{*s*}) with PetroOrg software.^{63,64} Heteroatom class (N_{*n*}O_{*o*}S_{*s*}), double bond equivalents (DBE = number of rings plus double bonds to carbon), and carbon number (C) were tabulated with relative abundance to aid in data visualization

Multivariate Analysis. Principal component analysis (PCA) was performed by PetroOrg with a nonlinear iterative partial least-squares (NIPALS) algorithm.^{65,66} The relative abundances for the six most abundant heteroatom classes (N₁, S₁, S₂, O₁S₁, HC, and radical HC) were loaded as variables into the input data matrix, with zero-filling applied for missed variables.⁶⁷ The principal components were assigned according to the percent of explained variance between the samples.

Table 2. Percent Elemental Composition of Carbon, Hydrogen, Nitrogen, Oxygen, and Sulfur in the Samples, Determined by Bulk Elemental Analysis

	GC645 reservoir	Mega Plume oil seep	Mega Plume oil slick	B-Day Candles oil slick	MC252 reservoir
C (%)	78.3 ± 0.9	84.1 ± 0.5	84.4 ± 0.1	84.3 ± 0.1	74.5 ± 0.6
H (%)	11.1 ± 0.2	11.2 ± 0.1	11.36 ± 0.03	11.10 ± 0.02	10.8 ± 0.1
N (%)	0.27 ± 0.01	0.29 ± 0.02	0.30 ± 0.02	0.33 ± 0.01	0.21 ± 0.01
O (%)	0.61 ± 0.03	0.96 ± 0.07	1.55 ± 0.03	1.79 ± 0.03	0.59 ± 0.06
S (%)	2.0 ± 0.1	2.48 ± 0.08	2.7 ± 0.2	2.82 ± 0.05	0.27 ± 0.01

GC/APCI-MS/MS of Mega Plume Oil Seep (Depth: 1220m) Hopanes: Summed Signals for C₂₇-C₃₅ (M⁺ → m/z 191)

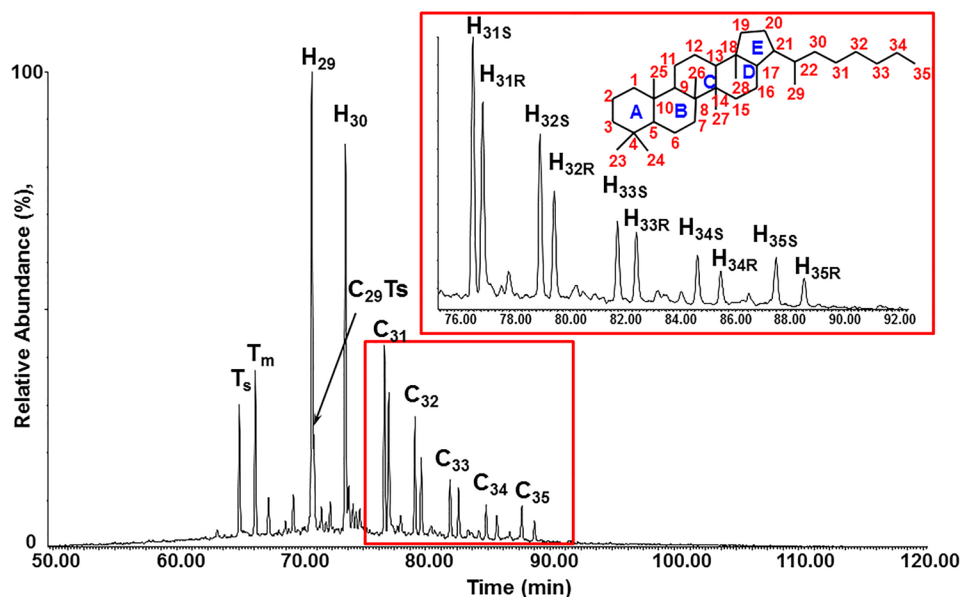


Figure 2. Sum of single reaction monitoring (SRM) transitions (M⁺ → m/z 191) for C₂₇–C₃₅ hopanes from the GC/APCI-MS/MS chromatogram for the Mega Plume oil seep sample.

RESULTS AND DISCUSSION

Bulk Elemental Analysis. The percent compositions of C, H, N, O, and S for each of the samples are listed in Table 2 after triplicate analysis. For the Mega Plume seep, surface slick, and Birthday Candles surface slick, approximately 100% of the sample composition was determined, versus only ~92% and ~86% for Holstein and MC252 reservoir crudes. Notably, the elemental composition determined for the MC252 crude is significantly different than previously reported in the literature, in which Macondo crude is reported to be 86.6% C, 12.6% H, 0.38% N, and 0.39% O.⁶⁸ Elemental analysis was performed by the combustion of the sample preweighed in a tin cup; however, that technique results in the loss of volatile components before measurement. Alternative analysis techniques (i.e., liquid injection) can minimize the loss of volatiles in elemental analysis and should be employed if available for use. Because the Holstein and MC252 are reservoir crudes, they contain volatile material, which explains the ~10+% imbalance in total composition. The field samples (Mega Plume seep, surface slick, and Birthday Candles surface slick) have already lost their volatiles before collection, and the elemental analysis technique selected was sufficient. It should be noted that the H/C ratios for the MC252 sample are similar to those previously reported. The H/C ratios for the reservoir crude are both higher, suggesting a more aromatic character than the H/C ratios for the field samples, whose lower H/C ratios suggest a more aromatic character. Aliphatic species are more likely to be volatile (i.e., fully lost in the field samples) and are favorably environmentally degraded over aromatic species, accounting for the H/C ratio differences determined between the reservoir and field samples.

Similarly, the oxygen content of the field samples is significantly higher than those of the GC645 and MC252 reservoir oils (~1–2% versus <0.60%) and reflects the environmental exposure of the Mega Plume and Birthday Candle samples compared to the reservoir crudes. Oxygenation

from biodegradation and photo-oxidation as the sample floats on the sea surface could account for the differences seen between surface slick samples and reservoir samples as well as oxygen concentration enrichment as lighter, more volatile hydrocarbons evaporate at the surface. The lack of information on time frame for exposure of samples in the environment before collection precludes quantitative data interpretation. Nevertheless, the greater oxygen content of the Birthday Candles surface slick sample suggests that the oil from that slick floated on the ocean surface longer than the Mega Plume surface slick prior to sampling. On the basis of chemical analysis, the Mega Plume oil seep sample understandably experienced the least environmental exposure, likely only to bacteria found around the oil vent with minimal photooxidation from sunlight.

The GC645 reservoir oil sample, Mega Plume oil seep, surface slick samples, and Birthday Candles surface slick sample all show higher levels of N and particularly S than the MC252 reservoir oil sample. Although weathering often results in oxygenation (e.g., photooxidation, biodegradation), N and S incorporation is rare. Therefore, the GC645 reservoir oil's sour (high sulfur) nature likely derives from the source material of the reservoir, rather than from environmental alterations as petroleum migrates in the subsurface or the water column. Because this sour character is detected in the Mega Plume and Birthday Candles samples, they are likely sourced from the GC645.

Chemical Fingerprinting Based on Petroleum Biomarkers. Bulk elemental analysis is readily affected by environmental transformations of the oil through biotic (biodegradation) and abiotic (e.g., dissolution, photooxidation, and evaporation) changes. Moreover, GC/(APCI)-MS/MS analysis is a powerful tool for fingerprinting crude oils and identifying the oil spill source and remains the traditional technique of choice.⁵² The fingerprinting of samples in this case is based on a trace analysis of petroleum biomarkers (steranes, diasteranes, and pentacyclic triterpanes) that naturally occur in crude oil and are highly resistant to environmental degradation.⁶⁹

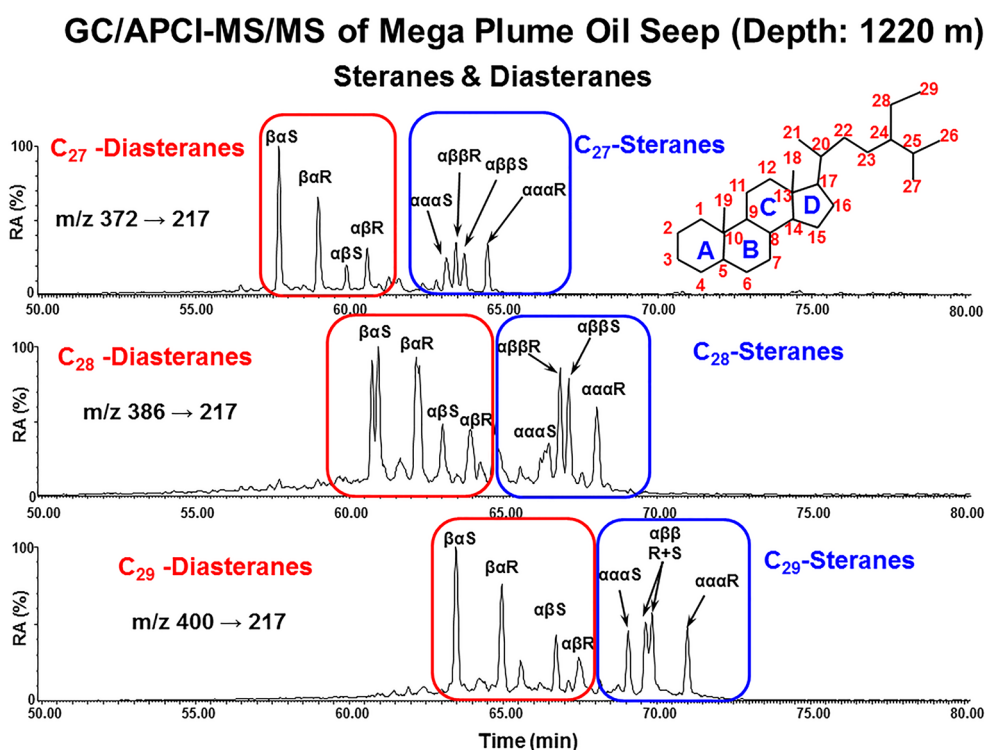


Figure 3. C_{27} – C_{29} sterane distribution for the Mega Plume oil seep sample from GC/APCI-MS/MS chromatograms (SRMs). Note the truncated labels corresponding to compounds described in the text. The number of carbon atoms in diasteranes and steranes is defined in each SRM chromatogram.

Figure 2 shows a gas chromatogram for a summed signal derived from nine SRM transitions for C_{27} – C_{35} triterpanes ($M^{+\bullet} \rightarrow m/z$ 191) in the Mega Plume oil seep, with assignment of more than a dozen hopanes: T_s , T_m , H_{29} , $C_{29}T_s$, H_{30} , H_{31S} , H_{31R} , H_{32S} , H_{32R} , H_{33S} , H_{33R} , H_{34S} , H_{34R} , H_{35S} , and H_{35R} (see SI for full compound names).

Steranes and diasteranes provide reliable sample identification. However, the coelution of steranes and diasteranes produces a challenge for their reliable assignment and integration without MS/MS capabilities. Thus, individual SRM transitions ($M^{+\bullet} \rightarrow m/z$ 217) facilitate assignment and integration of the peaks. Figure 3 shows chromatograms for each individual SRM transition for C_{27} – C_{29} steranes/diasteranes ($M^{+\bullet} \rightarrow m/z$ 217). We identified two dozen steranes and diasteranes: $C_{27}\beta\alpha S$, $C_{27}\beta\alpha R$, $C_{27}\alpha\beta S$, $C_{27}\alpha\beta R$, $C_{27}\alpha\alpha S$, $C_{27}\alpha\beta\beta R$, $C_{27}\alpha\beta\beta S$, $C_{27}\alpha\alpha R$, $C_{28}\beta\alpha S$, $C_{28}\beta\alpha R$, $C_{28}\alpha\beta S$, $C_{28}\alpha\beta R$, $C_{28}\alpha\alpha S$, $C_{28}\alpha\beta\beta R$, $C_{28}\alpha\beta\beta S$, $C_{28}\alpha\alpha R$, $C_{29}\beta\alpha S$, $C_{29}\beta\alpha R$, $C_{29}\alpha\beta S$, $C_{29}\alpha\beta R$, $C_{29}\alpha\alpha S$, $C_{29}\alpha\beta\beta R$, $C_{29}\alpha\beta\beta S$, and $C_{29}\alpha\alpha R$ (see SI for full compound names). Additional SRM transitions ($M^{+\bullet} \rightarrow m/z$ 218, $M^{+\bullet} \rightarrow m/z$ 259) specific for steranes and diasteranes (added to the experiment script, see Table S1) were used to increase confidence in the assignment of chromatographic peaks. In addition to selective SRM transitions, assignment of the peaks was also based on the elution order of hopanes, steranes, and diasteranes and retention times of hopanes and steranes in the NIST2266 standard.

Diagnostic biomarker ratios (rather than quantitative data for individual biomarkers) are usually reported in environmental and geochemical studies. Their utilization minimizes concentration effects of individual compounds caused by the samples (e.g., environmental changes, sample preparation, etc.) and levels out variations in routine instrument operation. Therefore, comparison of diagnostic ratios directly reflects differences in the target biomarker distribution among samples.⁷⁰ The petroleum

biomarkers identified in the Mega Plume oil seep sample were also found in all of the samples. In the current work, we consider seven diagnostic ratios (T_s/T_m , H_{29}/H_{30} , H_{31S}/H_{31R} , H_{32S}/H_{32R} , $H_{30}/(H_{31}+H_{32}+H_{33}+H_{34}+H_{35})$, $C_{27}\alpha\beta\beta/C_{29}\alpha\beta\beta$ steranes, and $C_{27}\beta\alpha/C_{29}\beta\alpha$ diasteranes), most of which were successfully used previously for fingerprinting and identification of chemical constituents of the Macondo oil spill.⁵²

Table S2 lists the biomarker ratios for all of the present samples. The calculated values are based on chromatographic peak areas. Reproducibility of the analytical method was confirmed by triplicate analysis, and relative standard deviation was within 14%. Spider diagrams constructed from the biomarker ratios for each sample facilitate data visualization (Figure 4, top). The Mega Plume oil seep, GC645 reservoir oil, and Mega Plume/Birthday Candles surface oil slicks samples all show close overlap across all seven biomarker ratios. The MC252 reservoir oil, however, has a noticeably larger T_s/T_m ratio and a smaller H_{29}/H_{30} ratio than the other four samples, and a slightly larger $H_{30}/(H_{31}+H_{32}+H_{33}+H_{34}+H_{35})$ ratio. For a more quantitative comparison, correlation coefficients for the samples relative to the Mega Plume oil seep sample were generated (Figure 4, bottom). In that assessment, the correlation of Mega Plume oil seep sample with itself is equal to one, and a correlation coefficient closer to one indicates greater similarity to the Mega Plume oil seep sample. The GC645 reservoir oil, Mega Plume oil slick, and Birthday Candles oil slick all demonstrate close similarity to the Mega Plume oil seep sample, with correlation coefficients greater than 0.95. It should also be noted that postseepage weathering of the Mega Plume sample collected on the sea surface did not significantly reduce the correlation to the sample collected at the seep site. Thus, we believe that the composition of the Birthday Candles slick sample collected on the sea surface is similar to that for the Birthday Candles seep on the ocean floor, for which no corresponding sample was available.

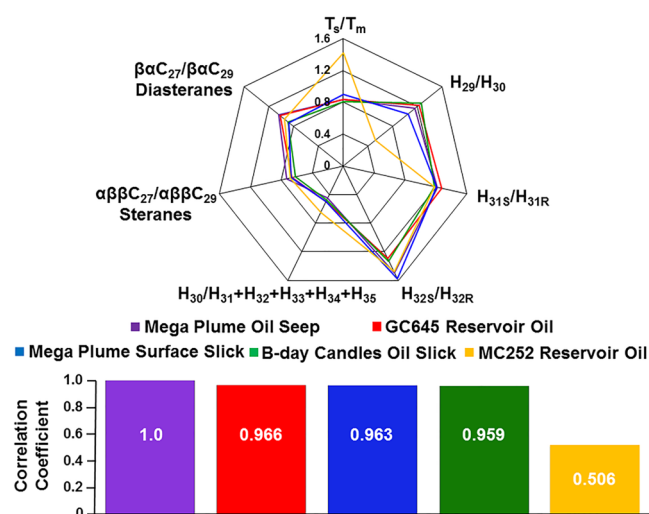


Figure 4. Spider diagram for seven common biomarker ratios in the samples, determined by APGC (top). Bottom: Correlation analysis of the biomarker ratios, comparing the samples to Mega Plume Oil Seep, with 1 signifying a perfect match. Mega Plume Oil Slick, B-day Candles Oil Slick, and GC645 Reservoir Oil all have high correlation to Megaplume Oil Seep, whereas Macondo Reservoir Oil exhibits a low correlation.

In contrast, the MC252 crude oil demonstrates a much lower correlation coefficient of 0.506, i.e., significantly different from all other samples. The biomarker analysis provides clear indication that the GC600/GC645 samples have a common source that differs from the Macondo reservoir 300 km away, thereby verifying our expected hypothesis.

FT-ICR MS Analysis. Gas chromatography limits the detectable molecules in GC/APCI-MS to those containing less than ~ 40 carbons. We therefore used FT-ICR MS to extend the analytical window and observe higher-boiling molecules to aid in molecular characterization while also enabling determination of the connectivity between the samples. Because most of the samples have high hydrocarbon and sulfur content, we selected atmospheric pressure photoionization (APPI), which readily

ionizes aromatic compounds, including sulfur species such as thiophenes.⁷¹ Figure 5 shows the relative abundances for a select group of highly abundant heteroatom classes (assigned peaks grouped by heteroatom content) for each sample. The relative abundance of the hydrocarbon (i.e., no heteroatoms) class for the MC252 reservoir sample is more than twice that for all of the other samples and is the most abundant heteroatom class in this sample. For all of the other samples, the S_1 class was the most abundant, in accord with the bulk elemental analysis shown in Table 2. Moreover, the relatively abundant S_2 and S_3 compounds could be assigned for the GC600/GC645 samples, whereas the relative abundance of S_2 species was less than 1%, and no S_3 molecules were observed for the MC252 reservoir sample. All samples exhibited similar O_1 class abundance distributions, but, as for the sulfur classes, the relative abundance of higher O_x species for the MC252 reservoir oil sample drops off more rapidly than for the other samples. Among all heteroatom classes, the GC600/GC645 samples had the most similar relative abundances, whereas the hydrocarbon and N_1 classes exhibited the most variance between samples. Hydrocarbon relative abundance is higher for the Mega Plume site. APPI ionization preferentially ionizes aromatic hydrocarbons, molecules whose concentrations would be enriched if the sample was subjected to greater biodegradation (which results in the loss of aliphatic hydrocarbons). Conversely, the Mega Plume samples exhibit a lower nitrogen relative abundance, despite similar nitrogen content (Table 1). Lower nitrogen relative abundance could simply be a consequence of higher hydrocarbon signal.

Double Bond Equivalents vs Carbon Number Plots. To visualize all of the elemental compositions for a given heteroatom class, isoabundance-contoured plots of DBE versus carbon number of the assigned species within the class were generated (Figure 6). The degree of aromaticity increases along the y-axis, and molecular size increases along the x-axis. The DBE and carbon number ranges for the hydrocarbon class are similar across all five samples, with the greatest difference for the MC252 sample. The MC252 sample's DBE is lower (i.e., more aliphatic) relative to the GC600/GC635 samples.

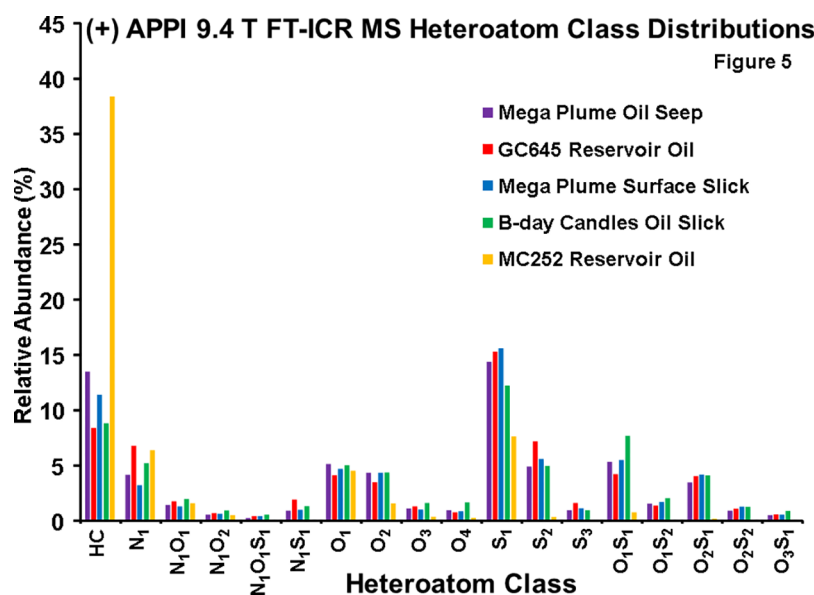


Figure 5. Heteroatom class relative abundance distributions, derived from (+) APPI 9.4 T FT-ICR MS analysis.

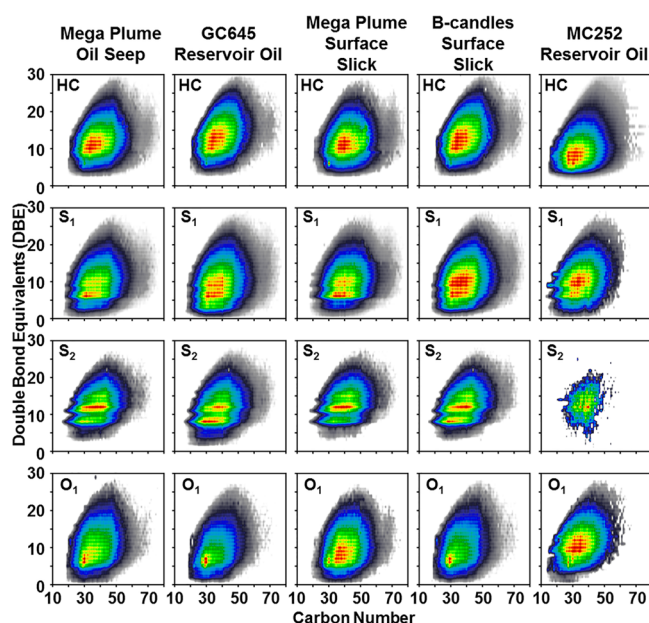


Figure 6. Isoabundance-contoured plots of double bond equivalents (DBE) vs carbon number for HC, S_1 , S_2 , and O_1 heteroatom classes from each of the five listed oil samples. Although all samples exhibit similar carbon number ranges for each class, the DBE ranges differ, most notably for the Macondo reservoir sample. The data are derived from (+) APPI 9.4 T FT-ICR mass spectra.

For the S_1 class, abundance distribution shows distinct peaks for DBE = 3, 6, and 9; corresponding to thiophene, benzothiophene, and dibenzothiophene derivatives, as commonly observed for sulfur species in crude oils.⁷² The Mega Plume oil seep and surface slick samples have highly abundant benzothiophenes and less abundant thiophenes and dibenzothiophenes, whereas the GC645 reservoir oil, Birthday Candles surface slick, and MC252 reservoir samples exhibit higher abundance in dibenzothiophenes, as well as thiophenes. For the S_2 class, the distinctive bands at DBE 8 and 11 are benzodithiophenes and dibenzodithiophenes. Due to the low class abundance, these bands are not detectable in the MC252 reservoir sample. The other four samples are all most abundant in dibenzodithiophenes, but the GC645 reservoir oil and Birthday Candles surface slick samples have a relatively higher abundance of benzodithiophenes than the Mega Plume samples. Because the Mega Plume samples are geographically farthest from the GC645 reservoir, chemical transformations affect benzodithiophene content as the petroleum migrates occur, although the specific reactions are unknown.

The O_1 heteroatom class for the Mega Plume oil seep, GC645 reservoir oil, and Birthday Candles surface slick sample each shows a similar abundance peak for DBE \approx 6, with a carbon number of \sim 28. These patterns are also seen in the Mega Plume surface slick sample, but in addition there is a range of highly abundant species that stretches from DBE 6–11 at higher carbon numbers. It is possible that this effect in the Mega Plume oil slick sample results from photooxidation of the oil on the sea surface, thereby generating additional O_1 species.

Relative Abundance vs DBE. To better visualize the DBE differences among the samples, we plotted the relative abundance of DBE for each of the six heteroatom classes for each of the samples in Figure 7. The relative abundance of the radical hydrocarbon class (top left) is much higher for the MC252 reservoir oil sample than for any of the other samples. In

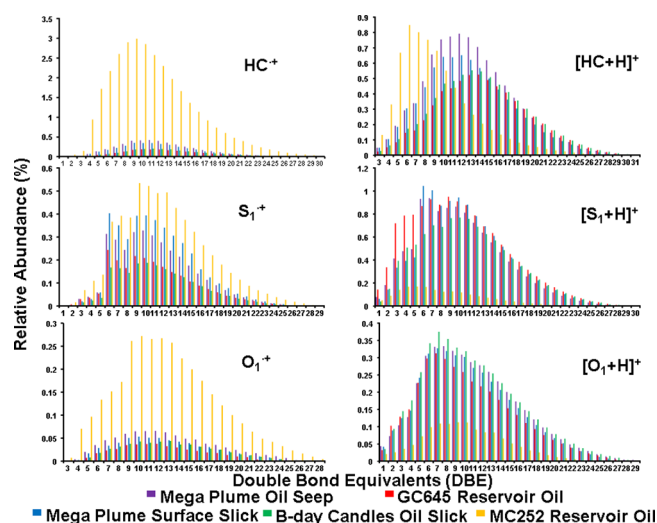


Figure 7. Relative abundance versus double bond equivalents (DBE) for HC, S_1 , and O_1 heteroatom classes, for each of five listed oil samples. Left: Molecular ions ($M^{+\bullet}$). Right: Protonated species ($[M+H]^+$). The Macondo oil (yellow) differs significantly from the others, suggesting a different reservoir source. The data are derived from (+) APPI 9.4 T FT-ICR mass spectra.

contrast, for the protonated hydrocarbons (top right), the relative abundance distribution for the MC252 reservoir sample is similar to those for the GC600/GC645 samples, but shifted to lower DBE (DBE \sim 6–7 versus \sim 12–14), due to the more aliphatic character of the MC252 reservoir oil. Note that the samples with the highest DBE (most aromatic) are the GC645 reservoir oil sample and the nearby (\sim 5 km NW) Birthday Candles oil slick sample. As the samples move further away from the GC645 reservoir (Mega Plume samples, \sim 1 km further NW) the DBE decreases and becomes more aliphatic.

The S_1 class (middle) diagrams clearly highlight the “steps” formed at DBE = 6 and 9 from benzothiophene and dibenzothiophene. Due to the low relative abundances at DBE = 3, a step for thiophenes is not apparent. For radical species (middle left), the DBE distributions are similar for all samples, but for protonated species (middle right), the MC252 reservoir oil sample exhibits far lower S_1 abundances, without the characteristic steps for the GC600/GC645 samples.

Finally, as for the hydrocarbons, a shift in as to which O_1 form (protonated or radical) is preferentially ionized is apparent between MC252 reservoir oil and the GC600/GC645 samples. The MC252 reservoir oil sample preferentially ionizes into radical O_1 species (bottom left), whereas all other samples preferentially ionize as protonated O_1 species (bottom right). A rationale for this observation is provided below (Principal Component Analysis section).

Principal Component Analysis. The first two principal components (PC1 and PC2) account for 98.83% of the total explained variance between the samples. Most (97.13%) of the variance is along the first principal component (PC1). Along that axis, MC252 reservoir oil is readily distinguished from all of the others (Figure 8, bottom). The loadings plot (Figure 8, top) indicates that the hydrocarbons detected as $M^{+\bullet}$ (radical HC class) are primarily responsible for the large negative difference in the MC252 reservoir oil versus the other four samples in accord with the differences in hydrocarbon class abundance seen in Figures 6 and 8. The main reason for the difference is the lower sulfur content of the MC252 reservoir sample. Both sulfur and

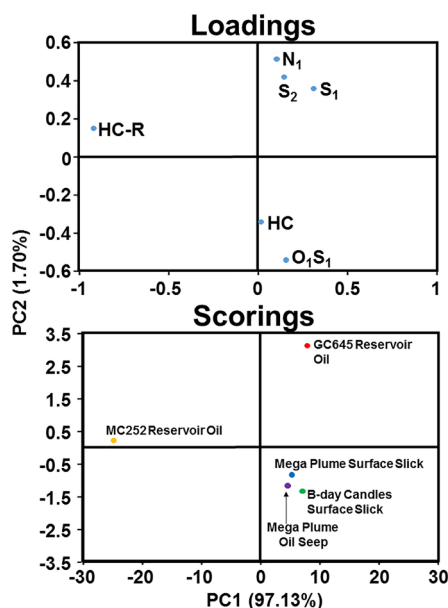


Figure 8. Principal component loadings (top) and scorings (bottom) plots derived from the relative abundances of the heteroatom classes indicated on the loadings chart. The loadings chart indicates the contribution from each heteroatom class. The scorings chart shows a clear separation of the Macondo reservoir oil from all of the other samples along the first principal component, which makes up 97.13% of the total variance. GC645 reservoir oil is separated from the others along the second principal component axis, which contributes only 1.70% of the total variance.

aromatic hydrocarbons are readily ionized by APPI; thus, a reduced sulfur content significantly increases the total relative abundance of the ionized hydrocarbons.

Among the other four samples, GC645 reservoir oil is primarily separated along the second principal component (PC2), which accounts for 1.70% of the data-explained variance, as a result of greater N_1 , S_1 , and S_2 versus HC and O_1S_1 relative abundances indicated by the loadings plot. The greater O_1S_1 relative abundance in the GC600 samples versus GC645 reservoir oil likely results from environmental oxidation of S_1 species as they made their way through the water column and sit exposed on the ocean surface. The HC class detected by APPI ionization is likely composed mainly of alkylated polycyclic aromatic hydrocarbons (PAHs). These PAHs are also present in higher concentration in the environmental samples, as evidenced from the H/C ratios derived from Table 2 as aliphatic carbon is degraded away. PC2, however, accounts for only a relatively small difference between the samples.

Implications. Throughout the data there is a consistent trend, in which the GC600 and GC645 samples differ from Macondo reservoir oil (MC252) based on bulk elemental composition, biomarker ratios, and relative abundance of ion classes from FT-ICR MS. Because MC252 was collected 300 km away, we conclude that it is geologically distinct from the GC600/GC645 samples, and that similarities between the others are the result of actual compositional similarities detected by the present methods. From the present results, we believe that petroleum from the GC645 reservoir is geologically linked to GC600, breaking through the sea floor through natural seeps such as Mega Plume and Birthday Candles, and forming oil slicks on the sea surface. The linkages between samples revealed by the present techniques provide a clear future pathway for future

study into petroleum migration, namely, how the oil is transformed, and thus integrated into the environment, as it travels. FT-ICR MS, through principal component analysis (PCA), demonstrates a clear relation between the GC600/GC645 samples not seen for the MC252 sample, which is verified by traditional biomarker analysis. FT-ICR MS further provides a path to more extensive molecular characterization, showing how chemical properties change (e.g., the petroleum appears to become more aromatic as it moves closer to the Mega Plume seep site and away from the GC645 reservoir, as well as changes in S character), whereas bulk elemental analysis demonstrates oxygen uptake of the petroleum at the seep site, sea surface, and the journey in between. A more intensive look into these chemical changes will provide a better understanding of the fate of petroleum in the environment.

■ ASSOCIATED CONTENT

Supporting Information

The Supporting Information is available free of charge on the ACS Publications website at DOI: 10.1021/acs.est.7b04445.

Full names of identified biomarkers abbreviated in the text; Table S1, the MS/MS conditions used for identifying various compound classes by GC/MS; and Table S2, the average value and standard deviation of the biomarker ratios after triplicate analysis displayed in Figure 4 (PDF)

■ AUTHOR INFORMATION

Corresponding Authors

*Phone: +1-(850)-345-4817. Fax: +1 850-644-0133. E-mail: lobodin@magnet.fsu.edu.

*Phone: +1-(850)-644-0529. Fax: +1 850-644-0133. E-mail: marshall@magnet.fsu.edu.

ORCID

Alan G. Marshall: 0000-0001-9375-2532

Notes

The authors declare no competing financial interest.

■ ACKNOWLEDGMENTS

The authors thank Ryan P. Rodgers for helpful discussions, Rebecca Ware for her assistance in elemental analysis, and Yuri E. Corilo for his assistance with software and chemometric analysis. This work was supported by NSF DMR-11-57490, BP/The Gulf of Mexico Research Initiative to the Deep-C Consortium, the Florida State University Future Fuels Institute, Waters Corporation, the State of Florida, NSF EF-0801741, and NSF OCE-1421180 (E.V.M.). Data are publicly available through the Gulf of Mexico Research Initiative Information & Data Cooperative (GRIIDC) at <https://data.gulfresearchinitiative.org>.

■ REFERENCES

- (1) Kvenvolden, K. A.; Cooper, C. K. Natural Seepage of Crude Oil into the Marine Environment. *Geo-Mar. Lett.* **2003**, *23* (3–4), 140–146.
- (2) National Research Council; Division on Earth and Life Studies; Transportation Research Board; Ocean Studies Board; Marine Board; Committee on Oil in the Sea: Inputs, Fates, and Effects. *Oil in the Sea III: Inputs, Fates, and Effects*; The National Academies Press: Washington, DC, 2003.
- (3) Prather, B. E. Calibration and Visualization of Depositional Process Models for above-Grade Slopes: A Case Study from the Gulf of Mexico. *Mar. Pet. Geol.* **2000**, *17* (5), 619–638.

- (4) Garcia-Pineda, O.; MacDonald, I.; Silva, M.; Shedd, W.; Daneshgar Asl, S.; Schumacher, B. Transience and Persistence of Natural Hydrocarbon Seepage in Mississippi Canyon, Gulf of Mexico. *Deep Sea Res., Part II* **2016**, *129*, 119–129.
- (5) Garcia-Pineda, O.; MacDonald, I.; Zimmer, B.; Shedd, B.; Roberts, H. Remote-Sensing Evaluation of Geophysical Anomaly Sites in the Outer Continental Slope, Northern Gulf of Mexico. *Deep Sea Res., Part II* **2010**, *57* (21–23), 1859–1869.
- (6) Macdonald, I. R.; Guinasso, N. L.; Ackleson, S. G.; Amos, J. F.; Duckworth, R.; Sassen, R.; Brooks, J. M. Natural Oil Slicks in the Gulf of Mexico Visible from Space. *J. Geophys. Res.* **1993**, *98* (C9), 16351–16364.
- (7) MacDonald, I. R.; Sager, W. W.; Peccini, M. B. Gas Hydrate and Chemosynthetic Biota in Mounded Bathymetry at Mid-Slope Hydrocarbon Seeps: Northern Gulf of Mexico. *Mar. Geol.* **2003**, *198*, 133–158.
- (8) Spies, R. B.; Davis, P. H.; Stuermer, D. H. *Elsevier Oceanogr. Ser.* **1980**, *27*, 229–263.
- (9) Reddy, C. M.; Arey, S. J.; Seewald, J. S.; Sylva, S. P.; Lemkau, K. L.; Nelson, R. K.; Carmichael, C. A.; McIntyre, C. P.; Fenwick, J.; Ventura, G. T.; Van Mooy, B. A. S.; Camilli, R. Composition and Fate of Gas and Oil Released to the Water Column during the Deepwater Horizon Oil Spill. *Proc. Natl. Acad. Sci. U. S. A.* **2012**, *109*, 20229–20234.
- (10) Orcutt, B. N.; Joye, S. B.; Kleindienst, S.; Knittel, K.; Ramette, A.; Reitz, A.; Samarkin, V.; Treude, T.; Boetius, A. Impact of Natural Oil and Higher Hydrocarbons on Microbial Diversity, Distribution, and Activity in Gulf of Mexico Cold-Seep Sediments. *Deep Sea Res., Part II* **2010**, *57* (21–23), 2008–2021.
- (11) Ziervogel, K.; D'souza, N.; Sweet, J.; Yan, B.; Passow, U. Natural Oil Slicks Fuel Surface Water Microbial Activities in the Northern Gulf of Mexico. *Front. Microbiol.* **2014**, *5*, DOI: [10.3389/fmicb.2014.00188](https://doi.org/10.3389/fmicb.2014.00188).
- (12) Kimes, N. E.; Callaghan, A. V.; Aktas, D. F.; Smith, W. L.; Sunner, J.; Golding, B. T.; Drozdowska, M.; Hazen, T. C.; Suflita, J. M.; Morris, P. J. Metagenomic Analysis and Metabolite Profiling of Deep-Sea Sediments from the Gulf of Mexico Following the Deepwater Horizon Oil Spill. *Front. Microbiol.* **2013**, *4*, DOI: [10.3389/fmicb.2013.00050](https://doi.org/10.3389/fmicb.2013.00050).
- (13) Fowler, S. W.; Knauer, G. A. Role of Large Particles in the Transport of Elements and Organic Compounds through the Oceanic Water Column. *Prog. Oceanogr.* **1986**, *16* (3), 147–194.
- (14) Atlas, R. M. Microbial Degradation of Petroleum Hydrocarbons: An Environmental Perspective. *Microbiol. Rev.* **1981**, *45* (1), 180–209.
- (15) Sassen, R.; MacDonald, I. R.; Requejo, A. G.; Guinasso, N. L.; Kennicutt, M. C.; Sweet, S. T.; Brooks, J. M. Organic Geochemistry of Sediments from Chemosynthetic Communities, Gulf of Mexico Slope. *Geo-Mar. Lett.* **1994**, *14* (2–3), 110–119.
- (16) MacDonald, I. R.; Bohrmann, G.; Escobar, E.; Abegg, F.; Blanchon, P.; Blinova, V.; Brueckmann, W.; Drews, M.; Eisenhauer, A.; Han, X.; Heeschen, K.; Meier, F.; Mortera, C.; Naehr, T.; Orcutt, B.; Bernard, B.; Brooks, J. M.; de Farago, M. Asphalt Volcanism and Chemosynthetic Life in the Campeche Knolls, Gulf of Mexico. *Science* **2004**, *304* (5673), 999–1002.
- (17) Barron, M. G. Ecological Impacts of the Deepwater Horizon Oil Spill: Implications for Immunotoxicity. *Toxicol. Pathol.* **2012**, *40* (2), 315–320.
- (18) Mendelssohn, I. A.; Andersen, G. L.; Baltz, D. M.; Caffey, R. H.; Carman, K. R.; Fleegeer, J. W.; Joye, S. B.; Lin, Q.; Maltby, E.; Overton, E. B.; Rozas, L. P. Oil Impacts on Coastal Wetlands: Implications for the Mississippi River Delta Ecosystem after the Deepwater Horizon Oil Spill. *BioScience* **2012**, *62* (6), 562–574.
- (19) Peterson, C. H.; Rice, S. D.; Short, J. W.; Esler, D.; Bodkin, J. K.; Ballachey, B. E.; Irons, D. B. Long-Term Ecosystem Response to the Exxon Valdez Oil Spill. *Science (Washington, DC, U. S.)* **2003**, *302* (5653), 2082–2086.
- (20) Macdonald, I. R.; Garcia-Pineda, O.; Beet, A.; Daneshgar Asl, S.; Feng, L.; Graettinger, G.; French-Mccay, D.; Holmes, J.; Hu, C.; Huffer, F.; Leifer, I.; Muller-Karger, F.; Solow, A.; Silva, M.; Swayze, G. Natural and Unnatural Oil Slicks in the Gulf of Mexico. *Journal of Geophysical Research: Oceans* **2015**, *120*, 8364.
- (21) Carvalho, G. de A.; Minnett, P. J.; Miranda, F. P. de; Landau, L.; Moreira, F. The Use of a RADARSAT-Derived Long-Term Dataset to Investigate the Sea Surface Expressions of Human-Related Oil Spills and Naturally Occurring Oil Seeps in Campeche Bay, Gulf of Mexico. *Can. J. Remote Sens.* **2016**, *42* (3), 307–321.
- (22) MacDonald, I. R.; Reilly, J. F., Jr.; Best, S. E.; Venkataramaiah, R.; Sassen, R.; Guinasso, N. L., Jr.; Amos, J. Remote Sensing Inventory of Active Oil Seeps and Chemosynthetic Communities in the Northern Gulf of Mexico. *Hydrocarbon Migration and Its near-Surface Expression: AAPG Memoir 66*; Schumacher, D., Abrams, M. A., Eds.; American Association of Petroleum Geologists, 1996; pp 27–37.
- (23) Brekke, C.; Solberg, A. H. S. Oil Spill Detection by Satellite Remote Sensing. *Remote Sens. Environ.* **2005**, *95* (1), 1–13.
- (24) Solberg, A. H. S.; Storvik, G.; Solberg, R.; Volden, E. Automatic Detection of Oil Spills in ERS SAR Images. *IEEE Trans. Geosci. Remote Sens.* **1999**, *37* (4), 1916–1924.
- (25) Fiscella, B.; Giancaspro, A.; Nirchio, F.; Pavese, P.; Trivero, P. Oil Spill Detection Using Marine SAR Images. *Int. J. Remote Sens.* **2000**, *21* (18), 3561–3566.
- (26) Johansen, C.; Todd, A. C.; MacDonald, I. R. Time Series Video Analysis of Bubble Release Processes at Natural Hydrocarbon Seeps in the Northern Gulf of Mexico. *Mar. Pet. Geol.* **2017**, *82*, 21–34.
- (27) De Beukelaer, S. M.; MacDonald, I. L.; Guinasso, N. L.; Murray, J. A. Distinct Side-Scan Sonar, RADARSAT SAR, and Acoustic Profiler Signatures of Gas and Oil Seeps on the Gulf of Mexico Slope. *Geo-Mar. Lett.* **2003**, *23* (3–4), 177–186.
- (28) Greinert, J.; Artemov, Y.; Egorov, V.; Debatist, M.; McGinnis, D. 1300-M-High Rising Bubbles from Mud Volcanoes at 2080m in the Black Sea: Hydroacoustic Characteristics and Temporal Variability. *Earth Planet. Sci. Lett.* **2006**, *244* (1–2), 1–15.
- (29) Merewether, R.; Olsson, M. S.; Lonsdale, P. Acoustically Detected Hydrocarbon Plumes Rising from 2-Km Depths in Guaymas Basin, Gulf of California. *J. Geophys. Res.* **1985**, *90* (B4), 3075.
- (30) Johansen, Ø.; Rye, H.; Cooper, C. DeepSpill—Field Study of a Simulated Oil and Gas Blowout in Deep Water. *Spill Sci. Technol. Bull.* **2003**, *8* (5), 433–443.
- (31) Grauls, D. Gas Hydrates: Importance and Applications in Petroleum Exploration. *Mar. Pet. Geol.* **2001**, *18* (4), 519–523.
- (32) Joye, S. B.; Boetius, A.; Orcutt, B. N.; Montoya, J. P.; Schulz, H. N.; Erickson, M. J.; Lugo, S. K. The Anaerobic Oxidation of Methane and Sulfate Reduction in Sediments from Gulf of Mexico Cold Seeps. *Chem. Geol.* **2004**, *205* (3–4), 219–238.
- (33) Stasiuk, L. D.; Snowdon, L. R. Fluorescence Micro-Spectrometry of Synthetic and Natural Hydrocarbon Fluid Inclusions: Crude Oil Chemistry, Density and Application to Petroleum Migration. *Appl. Geochem.* **1997**, *12* (3), 229–241.
- (34) Bodnar, R. J. Petroleum Migration in the Miocene Monterey Formation, California, USA: Constraints from Fluid-Inclusion Studies. *Mineral. Mag.* **1990**, *54* (375), 295–304.
- (35) Hood, K. C.; Wenger, L. M.; Gross, O. P.; Harrison, S. C. Hydrocarbon Systems Analysis of the Northern Gulf of Mexico: Delineation of Hydrocarbon Migration Pathways Using Seeps and Seismic Imaging. *AAPG Studies in Geology 48 and SEG Geophysical References Series No. 11, Surface Exploration case Histories: Applications of Geochemistry, Magnetism, and Remote Sensing*; Schumacher, D., LeSchack, L., Eds.; American Association of Petroleum Geologists, 2002.
- (36) Sassen, R.; Brooks, J. M.; Kennicutt, M. C., II; MacDonald, I. R.; Guinasso, N. L., Jr. How Oil Seeps, Discoveries Relate in Deepwater Gulf of Mexico. *Oil Gas J.* **1993**, *91* (16), 64–69.
- (37) Leahy, J. G.; Colwell, R. R. Microbial Degradation of Hydrocarbons in the Environment. *Microbiol. Rev.* **1990**, *54* (3), 305–315.
- (38) Tarr, M.; Zito, P.; Overton, E.; Olson, G.; Adkikari, P.; Reddy, C. Weathering of Oil Spilled in the Marine Environment. *Oceanography* **2016**, *29* (3), 126–135.
- (39) Dutta, T. K.; Harayama, S. Fate of Crude Oil by the Combination of Photooxidation and Biodegradation. *Environ. Sci. Technol.* **2000**, *34* (8), 1500–1505.
- (40) Sugiura, K.; Ishihara, M.; Shimauchi, T.; Harayama, S. Physicochemical Properties and Biodegradability of Crude Oil. *Environ. Sci. Technol.* **1997**, *31* (1), 45–51.

- (41) Espitalie, J.; Madec, M.; Tissot, B. Role of Mineral Matrix in Kerogen Pyrolysis; Influence on Petroleum Generation and Migration. *AAPG Bull.* **1980**, *64* (1), 59–LP-66.
- (42) Wardlaw, G. D.; Arey, J. S.; Reddy, C. M.; Nelson, R. K.; Ventura, G. T.; Valentine, D. L. Disentangling Oil Weathering at a Marine Seep Using GC × GC: Broad Metabolic Specificity Accompanies Subsurface Petroleum Biodegradation. *Environ. Sci. Technol.* **2008**, *42* (19), 7166–7173.
- (43) Wang, Z. Using Multiple Criteria for Fingerprinting Unknown Oil Samples Having Very Similar Chemical Composition. *Environ. Forensics* **2002**, *3* (3–4), 251–262.
- (44) Christensen, J. H.; Tomasi, G.; Hansen, A. B. Chemical Fingerprinting of Petroleum Biomarkers Using Time Warping and PCA. *Environ. Sci. Technol.* **2005**, *39* (1), 255–260.
- (45) Mulabagal, V.; Yin, F.; John, G. F.; Hayworth, J. S.; Clement, T. P. Chemical Fingerprinting of Petroleum Biomarkers in Deepwater Horizon Oil Spill Samples Collected from Alabama Shoreline. *Mar. Pollut. Bull.* **2013**, *70* (1–2), 147–154.
- (46) Stout, S.; Uhler, A.; McCarthy, K. A Strategy and Methodology for Defensibly Correlating Spilled Oil to Source Candidates. *Environ. Forensics* **2001**, *2* (1), 87–98.
- (47) Kujawinski, E. Electro Spray Ionization Fourier Transform Ion Cyclotron Resonance Mass Spectrometry (ESI FT-ICR MS): Characterization of Complex Environmental Mixtures. *Environ. Forensics* **2002**, *3* (3–4), 207–216.
- (48) Aeppli, C.; Carmichael, C. A.; Nelson, R. K.; Lemkau, K. L.; Graham, W. M.; Redmond, M. C.; Valentine, D. L.; Reddy, C. M. Oil Weathering after the Deepwater Horizon Disaster Led to the Formation of Oxygenated Residues. *Environ. Sci. Technol.* **2012**, *46* (16), 8799–8807.
- (49) Ray, P. Z.; Chen, H.; Podgorski, D. C.; McKenna, A. M.; Tarr, M. A. Sunlight Creates Oxygenated Species in Water-Soluble Fractions of Deepwater Horizon Oil. *J. Hazard. Mater.* **2014**, *280*, 636–643.
- (50) Marshall, A. G.; Hendrickson, C. L.; Jackson, G. S. Fourier Transform Ion Cyclotron Resonance Mass Spectrometry: A Primer. *Mass Spectrom. Rev.* **1998**, *17* (1), 1–35.
- (51) Rodgers, R. P.; Marshall, A. G. Petroleomics: Chemistry of the Underworld. *Proc. Natl. Acad. Sci. U. S. A.* **2008**, *105* (47), 18090.
- (52) Lobodin, V. V.; Maksimova, E. V.; Rodgers, R. P. Gas Chromatography/Atmospheric Pressure Chemical Ionization Tandem Mass Spectrometry for Fingerprinting the Macondo Oil Spill. *Anal. Chem.* **2016**, *88* (13), 6914–6922.
- (53) Jarvis, J. M.; McKenna, A. M.; Hilten, R. N.; Das, K. C.; Rodgers, R. P.; Marshall, A. G. Characterization of Pine Pellet and Peanut Hull Pyrolysis Bio-Oils by Negative-Ion Electro Spray Ionization Fourier Transform Ion Cyclotron Resonance Mass Spectrometry. *Energy Fuels* **2012**, *26* (6), 3810–3815.
- (54) Kaiser, N. K.; Quinn, J. P.; Blakney, G. T.; Hendrickson, C. L.; Marshall, A. G. A Novel 9.4 T FTICR Mass Spectrometer with Improved Sensitivity, Mass Resolution, and Mass Range. *J. Am. Soc. Mass Spectrom.* **2011**, *22* (8), 1343–1351.
- (55) Blakney, G. T.; Hendrickson, C. L.; Marshall, A. G. Predator Data Station: A Fast Data Acquisition System for Advanced FT-ICR MS Experiments. *Int. J. Mass Spectrom.* **2011**, *306* (2–3), 246–252.
- (56) Purcell, J. M.; Hendrickson, C. L.; Rodgers, R. P.; Marshall, A. G. Atmospheric Pressure Photoionization Fourier Transform Ion Cyclotron Resonance Mass Spectrometry for Complex Mixture Analysis. *Anal. Chem.* **2006**, *78* (16), S906–S912.
- (57) Tolmachev, A. V.; Robinson, E. W.; Wu, S.; Kang, H.; Lourette, N. M.; Pasa-Tolic, L.; Smith, R. D. Trapped-Ion Cell with Improved DC Potential Harmonicity for FT-ICR MS. *J. Am. Soc. Mass Spectrom.* **2008**, *19* (4), 586–597.
- (58) Kaiser, N. K.; Savory, J. J.; McKenna, A. M.; Quinn, J. P.; Hendrickson, C. L.; Marshall, A. G. Electrically Compensated Fourier Transform Ion Cyclotron Resonance Cell for Complex Mixture Mass Analysis. *Anal. Chem.* **2011**, *83* (17), 6907–6910.
- (59) Xian, F.; Hendrickson, C. L.; Blakney, G. T.; Beu, S. C.; Marshall, A. G. Automated Broadband Phase Correction of Fourier Transform Ion Cyclotron Resonance Mass Spectra. *Anal. Chem.* **2010**, *82* (21), 8807–8812.
- (60) Ledford, E. B., Jr.; Rempel, D. L.; Gross, M. L. Space Charge Effects in Fourier Transform Mass Spectrometry. *Mass Calibration. Anal. Chem.* **1984**, *56*, 2744–2748.
- (61) Shi, S. D.-H.; Drader, J. J.; Freitas, M. A.; Hendrickson, C. L.; Marshall, A. G. Comparison and Interconversion of the Two Most Common Frequency-to-Mass Calibration Functions for Fourier Transform Ion Cyclotron Resonance Mass Spectrometry. *Int. J. Mass Spectrom.* **2000**, *195-196*, 591–598.
- (62) Savory, J. J.; Kaiser, N. K.; McKenna, A. M.; Xian, F.; Blakney, G. T.; Rodgers, R. P.; Hendrickson, C. L.; Marshall, A. G. Parts-Per-Billion Fourier Transform Ion Cyclotron Resonance Mass Measurement Accuracy with a “Walking” Calibration Equation. *Anal. Chem.* **2011**, *83* (5), 1732–1736.
- (63) Hughey, C. A.; Hendrickson, C. L.; Rodgers, R. P.; Marshall, A. G.; Qian, K. Kendrick Mass Defect Spectroscopy: A Compact Visual Analysis for Ultrahigh-Resolution Broadband Mass Spectra. *Anal. Chem.* **2001**, *73*, 4676–4681.
- (64) Corilo, Y. E. *PetroOrg Software*; Florida State University; Tallahassee, FL.
- (65) Lohninger, H. *Teach/Me Data Analysis*; Springer: Berlin, 1999.
- (66) Esbensen, K. *Multivariate Analysis - in Practice*; CAMO Software Inc.: Woodbridge, NJ, 1998.
- (67) Hur, M.; Yeo, I.; Park, E.; Kim, Y. H.; Yoo, J.; Kim, E.; No, M.; Koh, J.; Kim, S. Combination of Statistical Methods and Fourier Transform Ion Cyclotron Resonance Mass Spectrometry for More Comprehensive, Molecular-Level Interpretations of Petroleum Samples. *Anal. Chem.* **2010**, *82* (1), 211–218.
- (68) Reddy, C. M.; Arey, J. S.; Seewald, J. S.; Sylva, S. P.; Lemkau, K. L.; Nelson, R. K.; Carmichael, C. A.; McIntyre, C. P.; Fenwick, J.; Ventura, G. T.; Van Mooy, B. A. S.; Camilli, R. Composition and Fate of Gas and Oil Released to the Water Column during the Deepwater Horizon Oil Spill. *Proc. Natl. Acad. Sci. U. S. A.* **2012**, *109*, 20229.
- (69) Wang, Z.; Stout, S. A. *Oil Spill Environmental Forensics: Fingerprinting and Source Identification*, 1st ed.; Academic Press, 2007.
- (70) Peters, K. E.; Walters, C. C.; Moldowan, J. M. I. Biomarkers and Isotopes in the Environment and Human History. *The Biomarker Guide*, 2nd ed.; Cambridge University Press: New York, 2005; Vol. 1.
- (71) Purcell, J. M.; Hendrickson, C. L.; Rodgers, R. P.; Marshall, A. G. Atmospheric Pressure Photoionization Proton Transfer for Complex Organic Mixtures Investigated by Fourier Transform Ion Cyclotron Resonance Mass Spectrometry. *J. Am. Soc. Mass Spectrom.* **2007**, *18* (9), 1682–1689.
- (72) Kim, E.-K.; No, M.-H.; Koh, J.-S.; Kim, S.-W. Compositional Characterization of Petroleum Heavy Oils Generated from Vacuum Distillation and Catalytic Cracking by Positive-Mode APPI FT-ICR Mass Spectrometry. *Mass Spectrom. Lett.* **2011**, *2* (2), 41–44.